

NOVEL QCD PHENOMENOLOGY

STANLEY J. BRODSKY*¹

¹*SLAC National Accelerator Laboratory
Stanford University, Stanford, California 94309
and CP³-Origins, Southern Denmark University
Odense, Denmark*

**E-mail: sjbth@slac.stanford.edu*

I review a number of topics where conventional wisdom in hadron physics has been challenged. For example, hadrons can be produced at large transverse momentum directly within a hard higher-twist QCD subprocess, rather than from jet fragmentation. Such “direct” processes can explain the deviations from perturbative QCD predictions in measurements of inclusive hadron cross sections at fixed $x_T = 2p_T/\sqrt{s}$, as well as the “baryon anomaly”, the anomalously large proton-to-pion ratio seen in high centrality heavy ion collisions. Initial-state and final-state interactions of the struck quark, the soft-gluon rescattering associated with its Wilson line, lead to Bjorken-scaling single-spin asymmetries, diffractive deep inelastic scattering, the breakdown of the Lam-Tung relation in Drell-Yan reactions, as well as nuclear shadowing and antishadowing. The Gribov-Glauber theory predicts that antishadowing of nuclear structure functions is not universal, but instead depends on the flavor quantum numbers of each quark and antiquark, thus explaining the anomalous nuclear dependence measured in deep-inelastic neutrino scattering. Since shadowing and antishadowing arise from the physics of leading-twist diffractive deep inelastic scattering, one cannot attribute such phenomena to the structure of the nucleus itself. It is thus important to distinguish “static” structure functions, the probability distributions computed from the square of the target light-front wavefunctions, versus “dynamical” structure functions which include the effects of the final-state rescattering of the struck quark. The importance of the $J = 0$ photon-quark QCD contact interaction in deeply virtual Compton scattering is also emphasized. The scheme-independent BLM method for setting the renormalization scale is discussed. Eliminating the renormalization scale ambiguity greatly improves the precision of QCD predictions and increases the sensitivity of searches for new physics at the LHC. Other novel features of QCD are discussed, including the consequences of confinement for quark and gluon condensates.

I. INTRODUCTION

Volodya Gribov, whose work we are honoring at this workshop, was never satisfied with conventional wisdom. In this contribution I will review a number of topics where new, and in some cases surprising, perspectives for QCD physics have emerged.

1. It is natural to assume that the nuclear modifications to the structure functions measured in deep inelastic lepton-nucleus and neutrino-nucleus interactions are identical; in fact, the Gribov-Glauber theory predicts that the antishadowing of nuclear structure functions is not universal, but depends on the quantum numbers of each struck quark and antiquark [1]. This observation can explain the recent analysis of Schienbein et al.[2] which shows that the NuTeV measurements of nuclear structure functions obtain from neutrino charged current reactions differ significantly from the distributions measured in deep inelastic electron and muon scattering.
2. It is conventional to assume that high transverse momentum hadrons in inclusive high energy hadronic collisions, such as $pp \rightarrow HX$, only arise from jet fragmentation. In fact, a significant fraction of high p_\perp^H events can emerge directly from a hard higher-twist subprocess [3, 4]. This phenomena can explain [5] the “baryon anomaly” observed at RHIC – the ratio of baryons to mesons at high p_\perp^H , as well as the power-law fall-off $1/p_\perp^n$ at fixed $x_\perp = 2p_\perp/\sqrt{s}$, both increase with centrality [6], opposite to the usual expectation that protons should suffer more energy loss in the nuclear medium than mesons.
3. The effects of final-state interactions of the scattered quark in deep inelastic scattering have been traditionally assumed to be power-law suppressed. In fact, the final-state gluonic interactions of the scattered quark lead to a T -odd non-zero spin correlation of the plane of the lepton-quark scattering plane with the polarization of the target proton [7]. This leading-twist Bjorken-scaling “Sivers effect” is nonuniversal since QCD predicts an opposite-sign correlation [8, 9] in Drell-Yan reactions due to the initial-state interactions of the annihilating antiquark. The same final-state interactions of the struck quark with the spectators [10] also lead to diffractive

events in deep inelastic scattering (DDIS) at leading twist, such as $\ell p \rightarrow \ell' p' X$, where the proton remains intact and isolated in rapidity; in fact, approximately 10% of the deep inelastic lepton-proton scattering events observed at HERA are diffractive [11, 12]. The presence of a rapidity gap between the target and diffractive system requires that the target remnant emerges in a color-singlet state; this is made possible in any gauge by the soft rescattering incorporated in the Wilson line or by augmented light-front wavefunctions [13].

4. It is usually assumed – following the intuition of the parton model – that the structure functions measured in deep inelastic scattering can be computed in the Bjorken-scaling leading-twist limit from the absolute square of the light-front wavefunctions, summed over all Fock states. In fact, dynamical effects, such as the Sivvers spin correlation and diffractive deep inelastic lepton scattering due to final-state gluon interactions, contribute to the experimentally observed DIS cross sections. Diffractive events also lead to the interference of two-step and one-step processes in nuclei which in turn, via the Gribov-Glauber theory, lead to the shadowing and the antishadowing of the deep inelastic nuclear structure functions [1]; such phenomena are not included in the light-front wavefunctions of the nuclear eigenstate. This leads to an important distinction between “dynamical” vs. “static” (wavefunction-specific) structure functions [14].
5. As noted by Collins and Qiu [15], the traditional factorization formalism of perturbative QCD fails in detail for many types of hard inclusive reactions because of initial- and final-state interactions. For example, if both the quark and antiquark in the Drell-Yan subprocess $q\bar{q} \rightarrow \mu^+\mu^-$ interact with the spectators of the other hadron, then one predicts a $\cos 2\phi \sin^2 \theta$ planar correlation in unpolarized Drell-Yan reactions [16]. This “double Boer-Mulders effect” can account for the large $\cos 2\phi$ correlation and the corresponding violation [16, 17] of the Lam Tung relation for Drell-Yan processes observed by the NA10 collaboration. An important signal for factorization breakdown at the LHC will be the observation of a $\cos 2\phi$ planar correlation in dijet production.
6. It is conventional to assume that the charm and bottom quarks in the proton structure functions only arise from gluon splitting $g \rightarrow Q\bar{Q}$. In fact, the proton light-front wavefunction contains *ab initio* intrinsic heavy quark Fock state components such as $|uudc\bar{c}\rangle$ [18–21]. The intrinsic heavy quarks carry most of the proton’s momentum since this minimizes the off-shellness of the state. The heavy quark pair $Q\bar{Q}$ in the intrinsic Fock state is primarily a color-octet, and the ratio of intrinsic charm to intrinsic bottom scales as $m_c^2/m_b^2 \simeq 1/10$, as can easily be seen from the operator product expansion in non-Abelian QCD [19, 21]. Intrinsic charm and bottom explain the origin of high x_F open-charm and open-bottom hadron production, as well as the single and double J/ψ hadroproduction cross sections observed at high x_F . The factorization-breaking nuclear $A^\alpha(x_F)$ dependence of hadronic J/ψ production cross sections is also explained. Kopeliovich, Schmidt, Soffer, Goldhaber, and I [22] have proposed a novel mechanism for Inclusive and diffractive Higgs production $pp \rightarrow pHp$ in which the Higgs boson carries a significant fraction of the projectile proton momentum. The production mechanism is based on the subprocess $(Q\bar{Q})g \rightarrow H$ where the $Q\bar{Q}$ in the $|uudQ\bar{Q}\rangle$ intrinsic heavy quark Fock state of the colliding proton has approximately 80% of the projectile protons momentum.
7. It is often stated that the renormalization scale of the QCD running coupling $\alpha_s(\mu_R^2)$ cannot be fixed, and thus it has to be chosen in an *ad hoc* fashion. In fact, as in QED, the scale can be fixed unambiguously by shifting μ_R so that all terms associated with the QCD β function vanish. In general, each set of skeleton diagrams has its respective scale. The result is independent of the choice of the initial renormalization scale μ_{R0} , thus satisfying Callan-Symanzik invariance. Unlike heuristic scale-setting procedures, the BLM method [23] gives results which are independent of the choice of renormalization scheme, as required by the transitivity property of the renormalization group. The divergent renormalon terms of order $\alpha_s^n \beta^n n!$ are transferred to the physics of the running coupling. Furthermore, one retains sensitivity to “conformal” effects which arise in higher orders, physical effects which are not associated with QCD renormalization. The BLM method also provides scale-fixed, scheme-independent high precision connections between observables, such as the “Generalized Crewther Relation” [24], as well as other “Commensurate Scale Relations” [25, 26]. Clearly the elimination of the renormalization scale ambiguity would greatly improve the precision of QCD predictions and increase the sensitivity of searches for new physics at the LHC.
8. It is usually assumed that the QCD coupling $\alpha_s(Q^2)$ diverges at $Q^2 = 0$; i.e., “infrared slavery”. In fact, determinations from lattice gauge theory, Bethe-Salpeter methods, effective charge measurements, gluon mass phenomena, and AdS/QCD all lead (in their respective scheme) to a finite value of the QCD coupling in the infrared [27]. Because of color confinement, the quark and gluon propagators vanish at long wavelength: $k < \Lambda_{QCD}$, and consequently the quantum loop corrections underlying the QCD β -function – decouple in the infrared, and the coupling freezes to a finite value at $Q^2 \rightarrow 0$ [28]. This observation underlies the use of conformal methods in AdS/QCD.

9. It is conventionally assumed that the vacuum of QCD contains quark $\langle 0|q\bar{q}|0 \rangle$ and gluon $\langle 0|G^{\mu\nu}G_{\mu\nu}|0 \rangle$ vacuum condensates, although the resulting vacuum energy density leads to a 10^{45} order-of-magnitude discrepancy with the measured cosmological constant. [29] However, a new perspective has emerged from Bethe-Salpeter and light-front analyses where the QCD condensates are identified as “in-hadron” condensates, rather than vacuum entities, but consistent with the Gell Mann-Oakes- Renner relation [30]. The “in-hadron” condensates become realized as higher Fock states of the hadron when the theory is quantized at fixed light-front time $\tau = x^0 + x^3/c$.
10. In nuclear physics nuclei are composites of nucleons. However, QCD provides a new perspective: [31, 32] six quarks in the fundamental 3_C representation of $SU(3)$ color can combine into five different color-singlet combinations, only one of which corresponds to a proton and neutron. The deuteron wavefunction is a proton-neutron bound state at large distances, but as the quark separation becomes smaller, QCD evolution due to gluon exchange introduces four other “hidden color” states into the deuteron wavefunction [33]. The normalization of the deuteron form factor observed at large Q^2 [34], as well as the presence of two mass scales in the scaling behavior of the reduced deuteron form factor [31], suggest sizable hidden-color Fock state contributions in the deuteron wavefunction [35]. The hidden-color states of the deuteron can be materialized at the hadron level as $\Delta^{++}(uuu)\Delta^-(ddd)$ and other novel quantum fluctuations of the deuteron. These dual hadronic components become important as one probes the deuteron at short distances, such as in exclusive reactions at large momentum transfer. For example, the ratio $d\sigma/dt(\gamma d \rightarrow \Delta^{++}\Delta^-)/d\sigma/dt(\gamma d \rightarrow np)$ is predicted to increase to a fixed ratio 2 : 5 with increasing transverse momentum p_T . Similarly, the Coulomb dissociation of the deuteron into various exclusive channels $ed \rightarrow e' + pn, pp\pi^-, \Delta\Delta, \dots$ will have a changing composition as the final-state hadrons are probed at high transverse momentum, reflecting the onset of hidden-color degrees of freedom.
11. It is usually assumed that the imaginary part of the deeply virtual Compton scattering amplitude is determined at leading twist by generalized parton distributions, but that the real part has an undetermined “ D -term” subtraction. In fact, the real part is determined by the local two-photon interactions of the quark current in the QCD light-front Hamiltonian [36, 37]. This contact interaction leads to a real energy-independent contribution to the DVCS amplitude which is independent of the photon virtuality at fixed t . The interference of the timelike DVCS amplitude with the Bethe-Heitler amplitude leads to a charge asymmetry in $\gamma p \rightarrow \ell^+\ell^-p$ [37–39]. Such measurements can verify that quarks carry the fundamental electromagnetic current within hadrons.
12. A long-sought goal in hadron physics is to find a simple analytic first approximation to QCD analogous to the Schrödinger-Coulomb equation of atomic physics. This problem is particularly challenging since the formalism must be relativistic, color-confining, and consistent with chiral symmetry. de Teramond and I have shown that the soft-wall AdS/QCD model, modified by a positive-sign dilaton metric, leads to a simple Schrödinger-like light-front wave equation and a remarkable one-parameter description of nonperturbative hadron dynamics [40–42]. The model predicts a zero-mass pion for zero-mass quarks and a Regge spectrum of linear trajectories with the same slope in the (leading) orbital angular momentum L of the hadrons and their radial quantum number N . Light-Front Holography maps the amplitudes which are functions of the fifth dimension variable z of anti-de Sitter space to a corresponding hadron theory quantized on the light front. The resulting Lorentz-invariant relativistic light-front wave equations are functions of an invariant impact variable ζ which measures the separation of the quark and gluonic constituents within the hadron at equal light-front time. The result is a semi-classical frame-independent first approximation to the spectra and light-front wavefunctions of meson and baryon light-quark bound states, which in turn predicts the behavior of the pion and nucleon form factors. The theory implements chiral symmetry in a novel way: the effects of chiral symmetry breaking increase as one goes toward large interquark separation, consistent with spectroscopic data, and the hadron eigenstates generally have components with different orbital angular momentum; e.g., the proton eigenstate in AdS/QCD with massless quarks has $L = 0$ and $L = 1$ light-front Fock components with equal probability. The AdS/QCD soft-wall model also predicts the form of the non-perturbative effective coupling $\alpha_s^{AdS}(Q)$ and its β -function, and the AdS/QCD light-front wavefunctions also lead to a method for computing the hadronization of quark and gluon jets at the amplitude level [43].

I will review several of these topics in these proceedings. Further discussion may be found in the references.

II. DIRECT PRODUCTION OF HIGH p_\perp HADRONS

A fundamental test of leading-twist QCD predictions in high transverse momentum hadronic reactions is the measurement of the power-law fall-off of the inclusive cross section [44] $Ed\sigma/d^3p(AB \rightarrow CX) = F(\theta_{cm}, x_T)/p_T^{n_{eff}}$ at fixed $x_T = 2p_T/\sqrt{s}$ and fixed θ_{CM} , where $n_{eff} \sim 4 + \delta$. Here $\delta = \mathcal{O}(1)$ is the correction to the conformal prediction

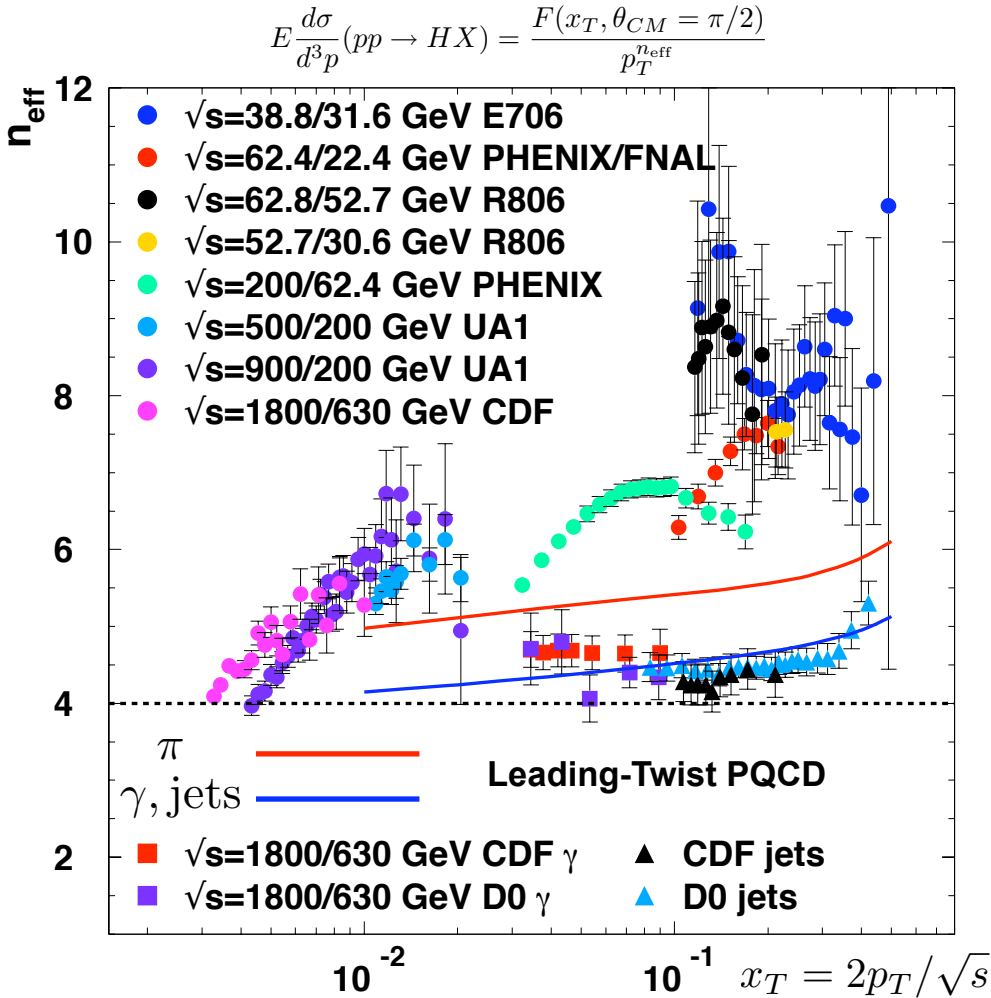


FIG. 1: Comparison of RHIC and fixed-target data for hadron, isolated photon, and jet production with the leading-twist pQCD predictions for the power-falloff of the semi-inclusive cross section $E d\sigma/d^3p(pp \rightarrow HX) = F(x_T, \theta_{CM} = \pi/2)/p_T^{n_{\text{eff}}}$ at fixed x_T . The data from R806, PHENIX, ISR/FNAL, E706 are for charged or neutral pion production, whereas the CDF, UA1 data at small x_T are for charged hadrons. The blue curve is the prediction of leading-twist QCD for isolated photon and jet production, including the scale-breaking effects of the running coupling and evolution of the proton structure functions. The red curve is the QCD prediction for pion production, which also includes the effect from the evolution of the fragmentation function. The dashed line at $n_{\text{eff}} = 4$ is the prediction of the scale-invariant parton model. From Arleo, et al. [3].

arising from the QCD running coupling and the DGLAP evolution of the input distribution and fragmentation functions [3, 4, 45]. The usual expectation is that leading-twist subprocesses will dominate measurements of high p_T hadron production at RHIC and Tevatron energies. Indeed, the data for isolated photon production $pp \rightarrow \gamma_{\text{direct}} X$ as well as jet production agrees well with the leading-twist scaling prediction $n_{\text{eff}} \simeq 4.5$ as seen in fig.1 [3]. However, as seen in fig.1, measurements of n_{eff} for $pp \rightarrow \pi X$ are not consistent with the leading twist predictions. Striking deviations from the leading-twist predictions were also observed at lower energy at the ISR and Fermilab fixed-target experiments [44, 46, 47]. The high values n_{eff} with x_T seen in the data indicate the presence of an array of higher-twist processes, including subprocesses where the hadron enters directly, rather than through jet fragmentation [48]. The predicted deviations for the experimental and NLO scaling exponent at RHIC and the LHC with PHENIX preliminary measurements are shown in fig. 2.

It should be emphasized that the existence of dynamical higher-twist processes in which a hadron interacts directly within a hard subprocess is a prediction of QCD. For example, the subprocess $\gamma^* q \rightarrow \pi q$, where the pion is produced directly through the pion's $\bar{q}q \rightarrow \pi$ distribution amplitude $\phi_\pi(x, Q)$ underlies deeply virtual meson scattering $\gamma p \rightarrow \pi X$. The corresponding timelike subprocess $\pi q \rightarrow \gamma^* q$ dominates the Drell-Yan reaction $\pi p \rightarrow \ell^+ \ell^- X$ at high x_F [49], thus

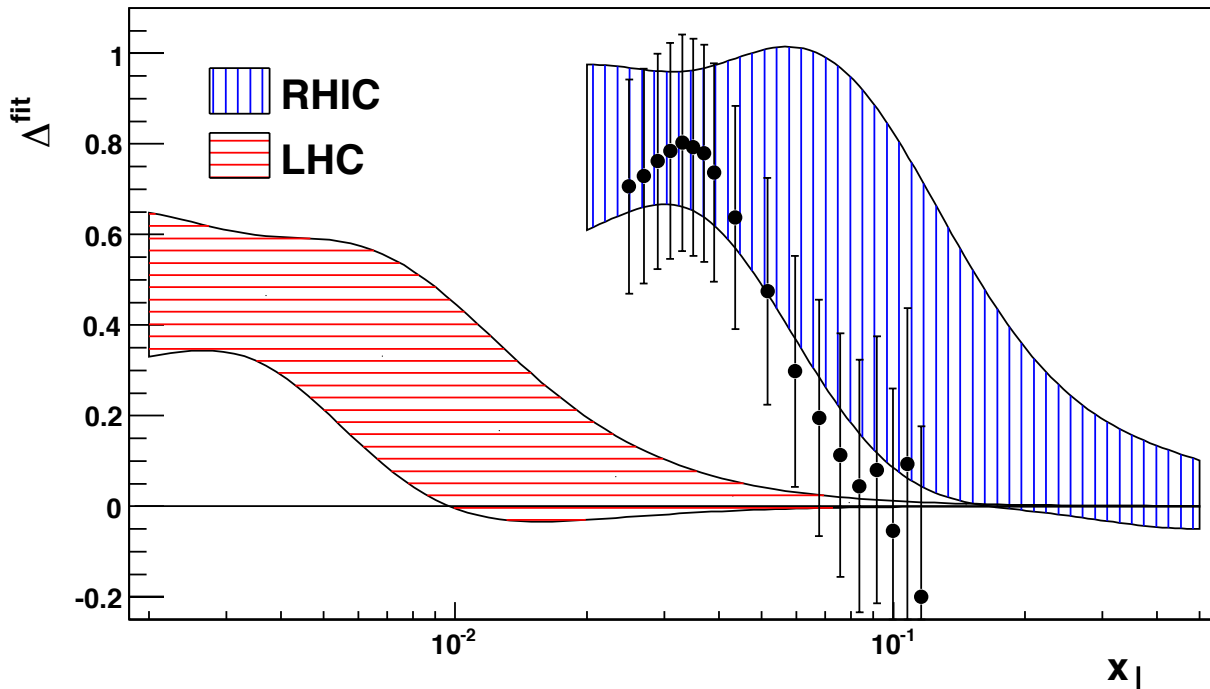


FIG. 2: Predicted difference between the experimental and NLO scaling exponent at RHIC ($\sqrt{s} = 200, 500$ GeV) and the LHC ($\sqrt{s} = 7$ TeV as compared to $\sqrt{s} = 1.8$ TeV), compared to PHENIX preliminary measurements. From Arleo, et al. [3].

accounting for the change in angular distribution from the canonical $1 + \cos^2 \theta$ distribution, for transversely polarized virtual photons, to $\sin^2 \theta$, corresponding to longitudinal photons; the virtual photon thus becomes longitudinally polarized at high x_F , reflecting the spin of the pion entering the direct QCD hard subprocess. Crossing predicts reactions where the final-state hadron appears directly in the subprocess such as $e^+e^- \rightarrow \pi X$ at $z = 1$. The nominal power-law fall-off at fixed x_T is set by the number of elementary fields entering the hard subprocess $n_{\text{eff}} = 2n_{\text{active}} - 4$. The power-law fall-off $(1 - x_T)^F$ at high x_T is set by the total number of spectators $F = 2n_{\text{spectators}} - 1$ [48], up to spin corrections.

The direct higher-twist subprocesses, where the trigger hadron is produced within the hard subprocess avoid the waste of same-side energy, thus allowing the target and projectile structure functions to be evaluated at the minimum values of x_1 and x_2 where they are at their maximum. Examples of direct baryon and meson higher-twist subprocesses are: $ud \rightarrow \Lambda \bar{s}, u\bar{d} \rightarrow \pi^+ g, ug \rightarrow \pi^+ d, u\bar{s} \rightarrow K^+ g, ug \rightarrow K^+ s$. These direct subprocesses involve the distribution amplitude of the hadron which has dimension Λ_{QCD} for mesons and Λ_{QCD}^2 for baryons; thus these higher-twist contributions to the inclusive cross section $Ed\sigma/d^3p$ at fixed x_T nominally scale as Λ_{QCD}^2/p_T^6 for mesons and Λ_{QCD}^4/p_T^8 for baryons.

The behavior of the single-particle inclusive cross section will be a key test of QCD at the LHC, since the leading-twist prediction for $n_{\text{eff}} \sim 4 + \delta$ is independent of the detailed form of the structure and fragmentation functions.

The fixed x_T scaling of the proton production cross section $Ed\sigma/d^3p(pp \rightarrow ppX)$ is particularly anomalous, far from the $1/p_T^4$ to $1/p_T^5$ scaling predicted by pQCD [45]. See fig.1. Sickles and I have argued that the anomalous features of inclusive high p_T proton production is due to hard subprocesses [45] where the proton is created directly within the hard reaction, such as $uu \rightarrow p\bar{d}$, such as the mechanism illustrated in fig.3. The fragmentation of a gluon or quark jet to a proton requires that the underlying 2 to 2 subprocess occurs at a higher transverse momentum than the p_T of the observed proton because of the fast-falling $(1 - z)^3$ quark-to-proton fragmentation function; in contrast, the direct subprocess is maximally energy efficient. Such “direct” reactions thus can explain the fast-falling power-law falloff observed at fixed x_T and fixed- θ_{cm} at the ISR, FermiLab and RHIC [45].

Since the proton is initially produced as a small-size $b_\perp \sim 1/p_T$ color-singlet state, it is “color transparent” [51], and it can thus propagate through dense nuclear matter with minimal energy loss. In contrast, the pions which are produced from jet fragmentation have a normal inelastic cross section. This provides a plausible explanation [5] of the RHIC data [6], which shows a dramatic rise of the p to π ratio with increasing p_T when one compares peripheral with central heavy ion collisions, as illustrated in fig.4. The color transparency of the proton produced in the direct

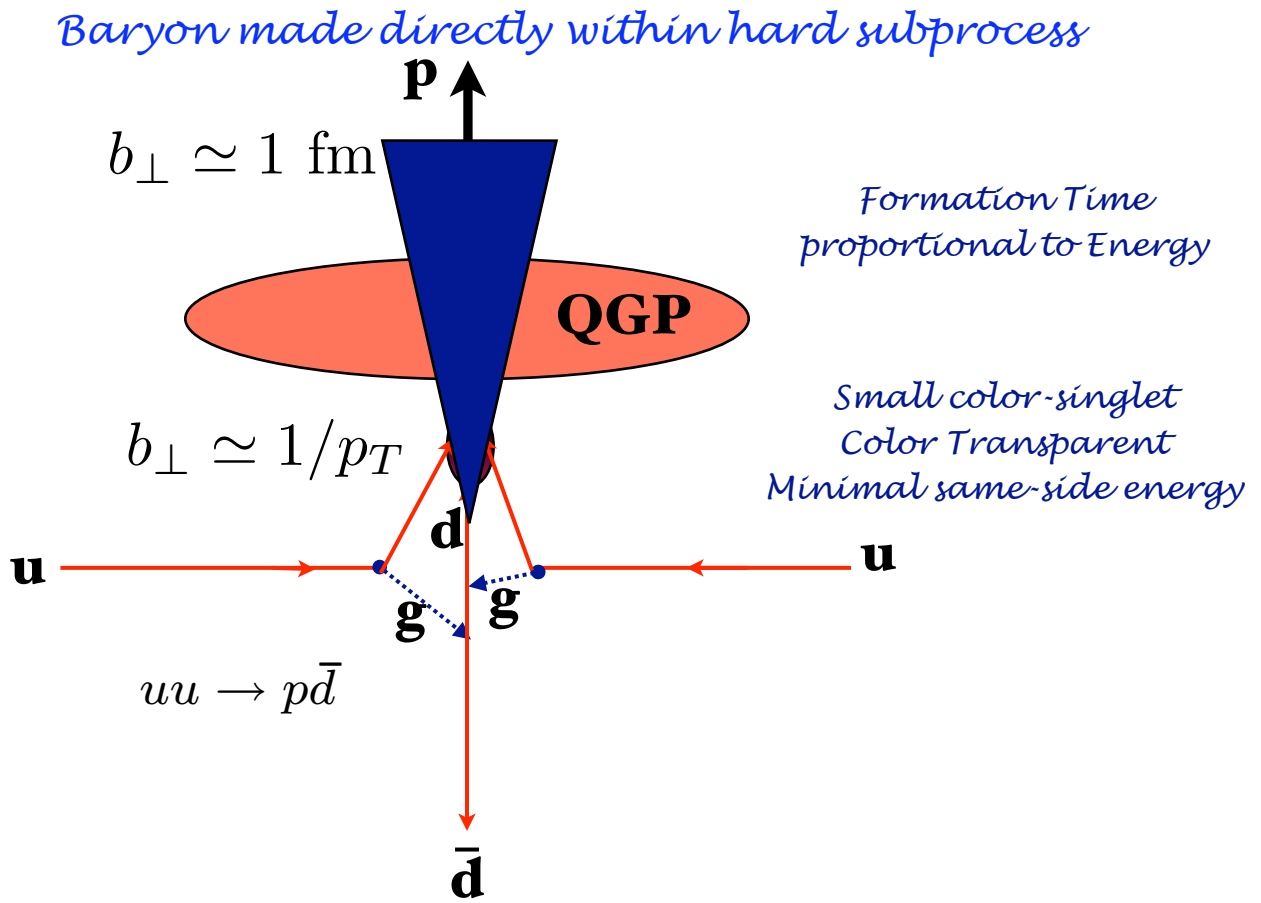


FIG. 3: Direct production of a proton in QCD. The proton is initially produced as a color-transparent small-size color singlet hadron.

process also can explain why the index n_{eff} rises with centrality, as seen in fig.5, – the higher-twist color-transparent subprocess dominates in the nuclear medium [45]. In addition, the fact that the proton tends to be produced alone in a direct subprocess explains why the yield of same-side hadrons along the proton trigger is diminished with increasing centrality. Thus the QCD color transparency of directly produced baryons can explain the baryon anomaly seen in heavy-ion collisions at RHIC: the color-transparent proton state is not absorbed, but a pion produced from fragmentation is diminished in the nuclear medium [50]. The increase of n_{eff} with centrality is consistent with the nuclear survival of direct higher-twist subprocesses for both protons and antiprotons, and to a lesser extent, for mesons.

III. LEADING-TWIST SHADOWING AND ANTI-SHADOWING OF NUCLEAR STRUCTURE FUNCTIONS

The shadowing of the nuclear structure functions: $R_A(x, Q^2) < 1$ at small $x < 0.1$ can be readily understood in terms of the Gribov-Glauber theory. Consider a two-step process in the nuclear target rest frame. The incoming $q\bar{q}$ dipole first interacts diffractively $\gamma^* N_1 \rightarrow (q\bar{q})N_1$ on nucleon N_1 leaving it intact. This is the leading-twist diffractive deep inelastic scattering (DDIS) process which has been measured at HERA to constitute approximately 10% of the DIS cross section at high energies. The $q\bar{q}$ state then interacts inelastically on a downstream nucleon N_2 : $(q\bar{q})N_2 \rightarrow X$. The phase of the pomeron-dominated DDIS amplitude is close to imaginary, and the Glauber cut provides another phase i , so that the two-step process has opposite phase and destructively interferes with the one-step DIS process

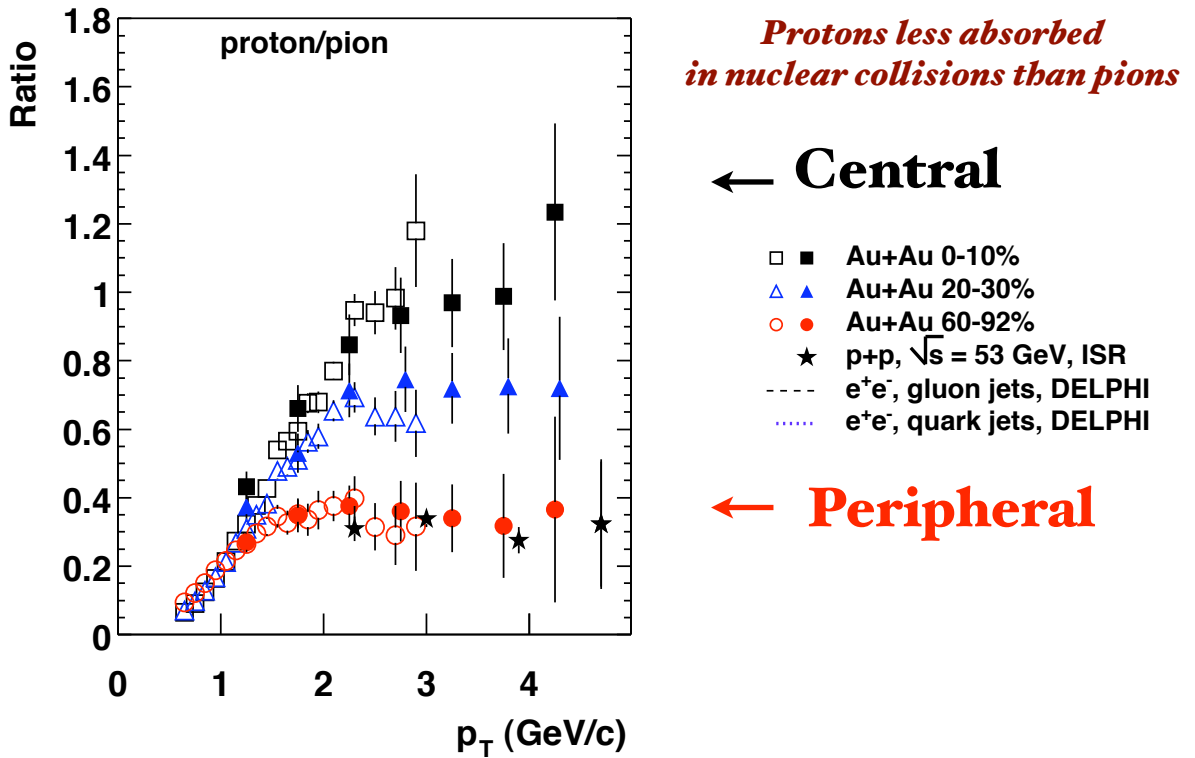
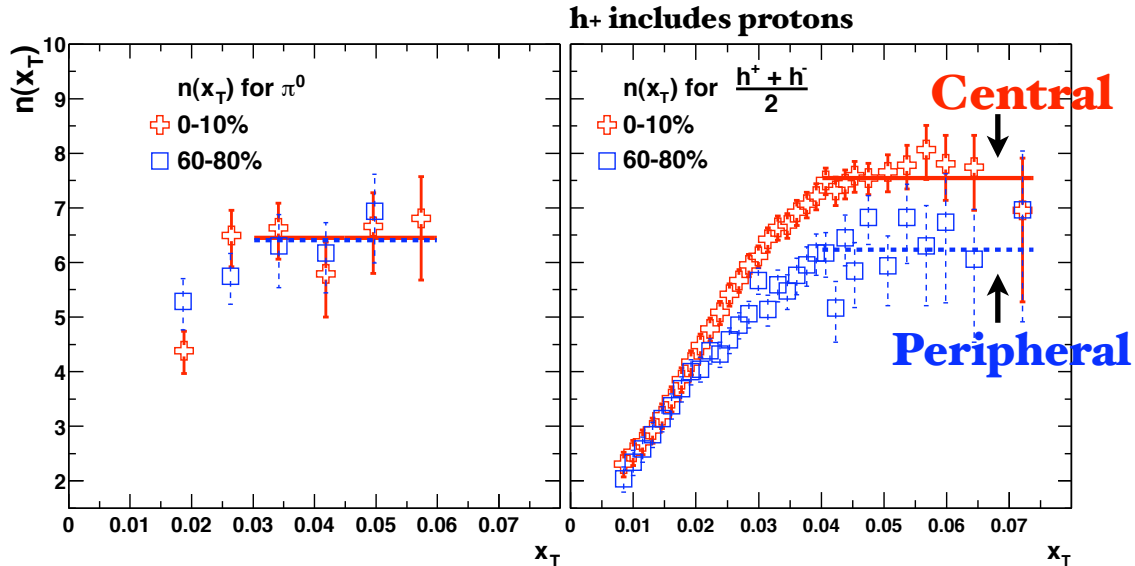


FIG. 4: The baryon anomaly observed by the PHENIX experiment at RHIC[6], The anomalous rise of the proton to pion ratio with centrality at large p_T .

$\gamma^* N_2 \rightarrow X$ where N_1 acts as an unscattered spectator. The one-step and two-step amplitudes can coherently interfere as long as the momentum transfer to the nucleon N_1 is sufficiently small that it remains in the nuclear target; *i.e.*, the Ioffe length [52] $L_I = 2M\nu/Q^2$ is large compared to the inter-nucleon separation. In effect, the flux reaching the interior nucleons is diminished, thus reducing the number of effective nucleons and $R_A(x, Q^2) < 1$. The Bjorken-scaling diffractive contribution to DIS arises from the rescattering of the struck quark after it is struck (in the parton model frame $q^+ \leq 0$), an effect induced by the Wilson line connecting the currents. Thus one cannot attribute DDIS to the physics of the target nucleon computed in isolation [10].

One of the novel features of QCD involving nuclei is the *antishadowing* of the nuclear structure functions as observed in deep inelastic lepton-nucleus scattering. Empirically, one finds $R_A(x, Q^2) \equiv (F_{2A}(x, Q^2)/(A/2)F_d(x, Q^2)) > 1$ in the domain $0.1 < x < 0.2$; *i.e.*, the measured nuclear structure function (referenced to the deuteron) is larger than the scattering on a set of A independent nucleons. Ivan Schmidt, Jian-Jun Yang, and I [1] have extended the analysis of nuclear shadowing to the shadowing and antishadowing of the electroweak structure functions. We note that there are leading-twist diffractive contributions $\gamma^* N_1 \rightarrow (q\bar{q})N_1$ arising from Reggeon exchanges in the t -channel [53]. For example, isospin-non-singlet $C = +$ Reggeons contribute to the difference of proton and neutron structure functions, giving the characteristic Kutzi-Weisskopf $F_{2p} - F_{2n} \sim x^{1-\alpha_R(0)} \sim x^{0.5}$ behavior at small x . The x dependence of the structure functions reflects the Regge behavior $\nu^{\alpha_R(0)}$ of the virtual Compton amplitude at fixed Q^2 and $t = 0$. The phase of the diffractive amplitude is determined by analyticity and crossing to be proportional to $-1 + i$ for $\alpha_R = 0.5$, which together with the phase from the Glauber cut, leads to *constructive* interference of the diffractive and nondiffractive multi-step nuclear amplitudes. The nuclear structure function is predicted to be enhanced precisely in the domain $0.1 < x < 0.2$ where antishadowing is empirically observed. The strength of the Reggeon amplitudes is



$$\sqrt{s_{NN}} = 130 \text{ and } 200 \text{ GeV}$$

FIG. 5: The power-law scaling index n_{eff} at fixed x_T as a function of centrality versus peripheral collisions, using spectra at $\sqrt{s} = 130$ GeV and $\sqrt{s} = 200$ GeV [50]. The positive-charged hadron trigger is dominated by protons at high p_T for central collisions, consistent with the color transparency of direct higher-twist baryon production processes.

fixed by the fits to the nucleon structure functions, so there is little model dependence. Since quarks of different flavors will couple to different Reggeons; this leads to the remarkable prediction that nuclear antishadowing is not universal; it depends on the quantum numbers of the struck quark. This picture implies substantially different antishadowing for charged and neutral current reactions, thus affecting the extraction of the weak-mixing angle θ_W . The ratio of nuclear to nucleon structure functions $R_{A/N}(x, Q) = \frac{F_{2A}(x, Q)}{AF_{2N}(x, Q)}$ is thus process independent. We have also identified contributions to the nuclear multi-step reactions which arise from odderon exchange and hidden color degrees of freedom in the nuclear wavefunction.

Schienbein et al. [2] have recently given a comprehensive analysis of charged current deep inelastic neutrino-iron scattering, finding significant differences with the nuclear corrections for electron-iron scattering. See fig.6. The measured nuclear effect measured in the NuTeV deep inelastic scattering charged current experiment is distinctly different from the nuclear modification measured at SLAC and NMC in deep inelastic scattering electron and muon scattering. This implies that part of the anomalous NuTeV result [54] for θ_W could be due to the non-universality of nuclear antishadowing for charged and neutral currents.

A new understanding of nuclear shadowing and antishadowing has emerged based on multi-step coherent reactions involving leading twist diffractive reactions [1, 53]. The nuclear shadowing of structure functions is a consequence of the lepton-nucleus collision; it is not an intrinsic property of the nuclear wavefunction. The same analysis shows that antishadowing is *not universal*, but it depends in detail on the flavor of the quark or antiquark constituent [1]. Detailed measurements of the nuclear dependence of individual quark structure functions are thus needed to establish the distinctive phenomenology of shadowing and antishadowing and to make the NuTeV results definitive. A comparison

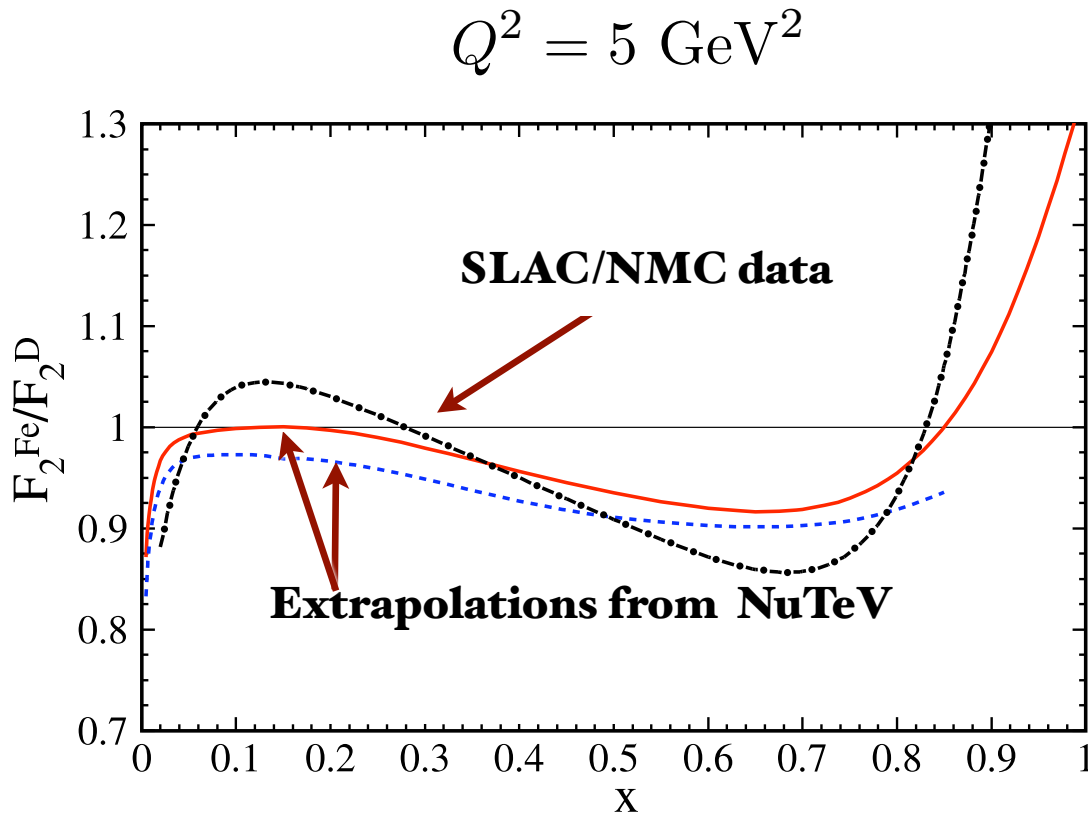


FIG. 6: Comparison of the Nuclear Modification of Charged vs. Neutral Current Deep Inelastic Structure Functions. From I. Schienbein et al. [2]

of the nuclear modification in neutrino versus anti-neutrino interactions is clearly important. There are other ways in which this new view of antishadowing can be tested; for example, antishadowing can also depend on the target and beam polarization.

IV. DYNAMIC VERSUS STATIC HADRONIC STRUCTURE FUNCTIONS

The nontrivial effects from rescattering and diffraction highlight the need for a fundamental understanding the dynamics of hadrons in QCD at the amplitude level. This is essential for understanding phenomena such as the quantum mechanics of hadron formation, the remarkable effects of initial and final interactions, the origins of diffractive phenomena and single-spin asymmetries, and manifestations of higher-twist semi-exclusive hadron subprocesses. A central tool in these analyses is the light-front wavefunctions of hadrons, the frame-independent eigensolutions of the Heisenberg equation for QCD $H^{LF}|\Psi\rangle = M^2|\Psi\rangle$ quantized at fixed light-front. Given the light-front wavefunctions $\psi_{n/H}(x_i, \vec{k}_{\perp i}, \lambda_i)$, one can compute a large range of exclusive and inclusive hadron observables. For example, the valence, sea-quark and gluon distributions are defined from the squares of the LFWFS summed over all Fock states n . Form factors, exclusive weak transition amplitudes [55] such as $B \rightarrow \ell\nu\pi$, and the generalized parton distributions [56] measured in deeply virtual Compton scattering are (assuming the “handbag” approximation) overlaps of the initial and final LFWFS with $n = n'$ and $n = n' + 2$.

It is thus important to distinguish “static” structure functions which are computed directly from the light-front

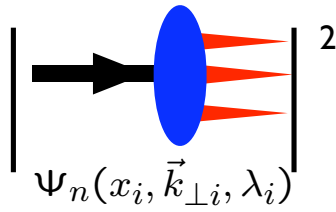
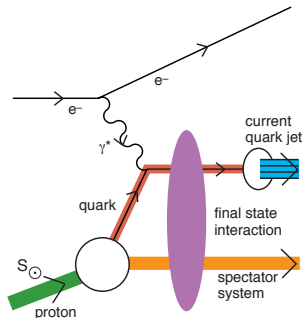
Static	Dynamic
<ul style="list-style-type: none"> • Square of Target LFWFs • No Wilson Line • Probability Distributions • Process-Independent • T-even Observables • No Shadowing, Anti-Shadowing • Sum Rules: Momentum and J^z • DGLAP Evolution; mod. at large x • No Diffractive DIS 	<p>Modified by Rescattering: ISI & FSI</p> <p>Contains Wilson Line, Phases</p> <p>No Probabilistic Interpretation</p> <p>Process-Dependent - From Collision</p> <p>T-Odd (Sivers, Boer-Mulders, etc.)</p> <p>Shadowing, Anti-Shadowing, Saturation</p> <p>Sum Rules Not Proven</p> <p>DGLAP Evolution</p> <p>Hard Pomeron and Odderon Diffractive DIS</p>
	

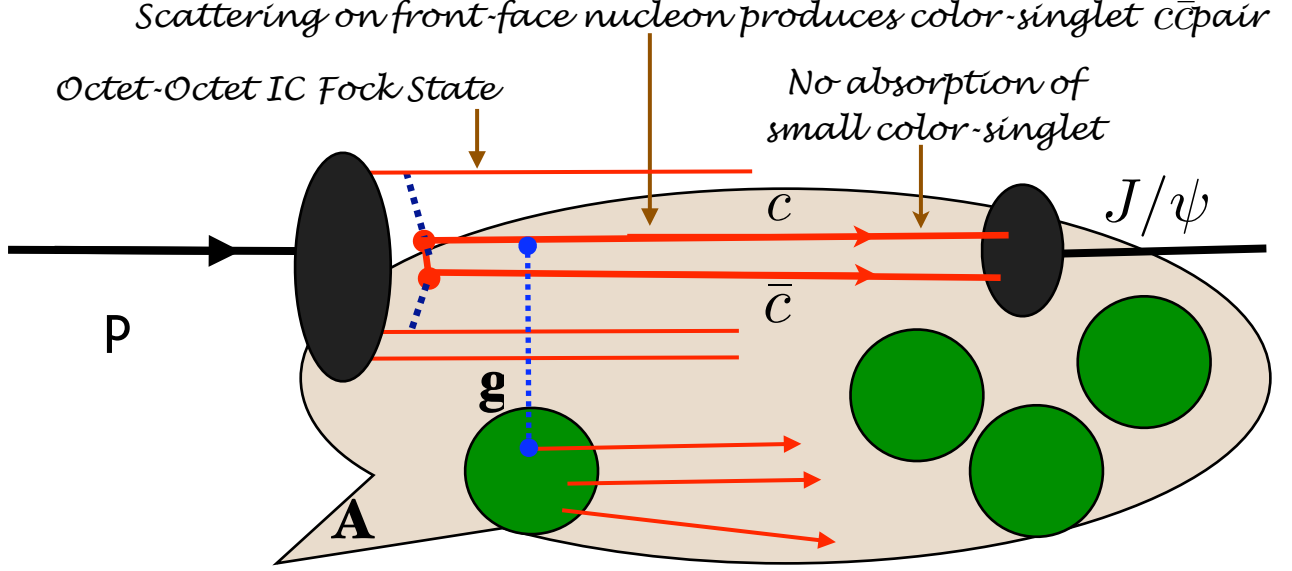
FIG. 7: Static versus dynamic structure functions

wavefunctions of a target hadron from the nonuniversal “dynamic” empirical structure functions which take into account rescattering of the struck quark in deep inelastic lepton scattering. See fig.7. The real wavefunctions underlying static structure functions cannot describe diffractive deep inelastic scattering nor single-spin asymmetries, since such phenomena involve the complex phase structure of the γ^*p amplitude. One can augment the light-front wavefunctions with a gauge link corresponding to an external field created by the virtual photon $q\bar{q}$ pair current [57, 58], but such a gauge link is process dependent [8], so the resulting augmented wavefunctions are not universal. [10, 57, 59]. The physics of rescattering and nuclear shadowing is not included in the nuclear light-front wavefunctions, and a probabilistic interpretation of the nuclear DIS cross section is precluded.

V. NOVEL INTRINSIC HEAVY QUARK PHENOMENA

Intrinsic heavy quark distributions are a rigorous feature of QCD, arising from diagrams in which two or more gluons couple the valence quarks to the heavy quarks. The probability for Fock states of a light hadron to have an extra heavy quark pair decreases as $1/m_Q^2$ in non-Abelian gauge theory [19, 21]. The relevant matrix element is the cube of the QCD field strength $G_{\mu\nu}^3$, in contrast to QED where the relevant operator is $F_{\mu\nu}^4$ and the probability of intrinsic heavy leptons in an atomic state is suppressed as $1/m_\ell^4$. The maximum probability occurs at $x_i = m_{\perp i} / \sum_{j=1}^n m_{\perp j}^j$ where $m_{\perp i} = \sqrt{k_{\perp i}^2 + m_i^2}$; *i.e.*, when the constituents have minimal invariant mass and equal rapidity. Thus the heaviest constituents have the highest momentum fractions and the highest x_i . Intrinsic charm thus predicts that the charm structure function has support at large x_{bj} in excess of DGLAP extrapolations [18]; this is in agreement with

*Color-Opaque IC Fock state
interacts on nuclear front surface*



$$\frac{d\sigma}{dx_F}(pA \rightarrow J/\psi X) = A^{2/3} \times \frac{d\sigma}{dx_F}(pN \rightarrow J/\psi X)$$

FIG. 8: Color-Octet intrinsic charm mechanism for the nuclear dependence of J/ψ production

the EMC measurements [20]. Intrinsic charm can also explain the $J/\psi \rightarrow \rho\pi$ puzzle [60]. It also affects the extraction of suppressed CKM matrix elements in B decays [61]. The dissociation of the intrinsic charm $|uudc\bar{c}\rangle$ Fock state of the proton can produce a leading heavy quarkonium state at high $x_F = x_c + x_{\bar{c}}$ in $pN \rightarrow J/\psi X$ since the c and \bar{c} can readily coalesce into the charmonium state. Since the constituents of a given intrinsic heavy-quark Fock state tend to have the same rapidity, coalescence of multiple partons from the projectile Fock state into charmed hadrons and mesons is also favored. For example, one can produce a leading Λ_c at high x_F and low p_T from the coalescence of the udc constituents of the projectile $|uudc\bar{c}\rangle$ Fock state.

The operator product analysis of the IC matrix element shows that the IC Fock state has a dominant color-octet structure: $|(uud)_{8C}(c\bar{c})_{8C}\rangle$. The color octet $c\bar{c}$ converts to a color singlet by gluon exchange on the front surface of a nuclear target and then coalesces to a J/ψ which interacts weakly through the nuclear volume [22]. Thus the rate for the IC component has $A^{2/3}$ dependence corresponding to the area of the front surface. This is illustrated in fig 8. This forward contribution is in addition to the A^1 contribution derived from the usual perturbative QCD fusion contribution at small x_F . Because of these two components, the cross section violates perturbative QCD factorization for hard inclusive reactions [62]. This is consistent with the two-component cross section for charmonium production observed by the NA3 collaboration at CERN [63] and more recent experiments [64]. The diffractive dissociation of the intrinsic charm Fock state leads to leading charm hadron production and fast charmonium production in agreement with measurements [65]. The hadroproduction cross sections for double-charm Ξ_{cc}^+ baryons at SELEX [66] and the production of J/ψ pairs at NA3 are consistent with the diffractive dissociation and coalescence of double IC Fock states [67]. These observations provide compelling evidence for the diffractive dissociation of complex off-shell Fock states of the projectile and contradict the traditional view that sea quarks and gluons are always produced

perturbatively via DGLAP evolution or gluon splitting. It is also conceivable that the observations [68] of Λ_b at high x_F at the ISR in high energy pp collisions could be due to the dissociation and coalescence of the “intrinsic bottom” $|uud\bar{b}\bar{b}\rangle$ Fock states of the proton.

As emphasized by Lai, Tung, and Pumplin [69], there are strong indications that the structure functions used to model charm and bottom quarks in the proton at large x_{bj} have been underestimated, since they ignore intrinsic heavy quark fluctuations of hadron wavefunctions. The anomalous growth of the $p\bar{p} \rightarrow \gamma cX$ inclusive cross section observed by D0 collaboration [70] at the Tevatron also indicates that the charm distribution has been underestimated at $x > 0/1$. Furthermore, the neglect of the intrinsic-heavy quark component in the proton structure function will lead to an incorrect assessment of the gluon distribution at large x if it is assumed that sea quarks always arise from gluon splitting. It is thus critical for new experiments (HERMES, HERA, COMPASS) to definitively establish the phenomenology of the charm structure function at large x_{bj} .

VI. VACUUM EFFECTS AND LIGHT-FRONT QUANTIZATION

The vacuum in quantum field theories is remarkably simple in light-cone quantization because of the restriction $k^+ \geq 0$. For example in QED, vacuum graphs such as $e^+e^-\gamma$ associated with the zero-point energy do not arise. In the Higgs theory, the usual Higgs vacuum expectation value is replaced with a $k^+ = 0$ zero mode; [71] however, the resulting phenomenology is identical to the standard analysis.

Hadronic condensates play an important role in quantum chromodynamics. It is widely held that quark and gluon vacuum condensates have a physical existence, independent of hadrons, measurable spacetime-independent configurations of QCD’s elementary degrees-of-freedom in a hadron-less ground state. However, a non-zero spacetime-independent QCD vacuum condensate poses a critical dilemma for gravitational interactions because it would lead to a cosmological constant some 45 orders of magnitude larger than observation. As noted in Ref. [29], this conflict is avoided if strong interaction condensates are properties of the light-front wavefunctions of the hadrons, rather than the hadron-less ground state of QCD.

The usual assumption that non-zero vacuum condensates exist and possess a measurable reality has long been recognized as posing a conundrum for the light-front formulation of QCD. In the light-front formulation, the ground-state is a structureless Fock space vacuum, in which case it would seem to follow that dynamical chiral symmetry breaking (CSB) is impossible. In fact, as first argued by Casher and Susskind [72] dynamical CSB must be a property of hadron wavefunctions, not of the vacuum in the light-front framework. This thesis has also been explored in a series of recent articles [28, 29, 43].

Conventionally, the quark and gluon condensates are considered to be properties of the QCD vacuum and hence to be constant throughout spacetime. A new perspective on the nature of QCD condensates $\langle \bar{q}q \rangle$ and $\langle G_{\mu\nu}G^{\mu\nu} \rangle$, particularly where they have spatial and temporal support, has recently been presented. [28–30, 73, 74] Their spatial support is restricted to the interior of hadrons, since these condensates arise due to the interactions of quarks and gluons which are confined within hadrons. For example, consider a meson consisting of a light quark q bound to a heavy antiquark, such as a B meson. One can analyze the propagation of the light q in the background field of the heavy \bar{b} quark. Solving the Dyson-Schwinger equation for the light quark one obtains a nonzero dynamical mass and, via the connection mentioned above, hence a nonzero value of the condensate $\langle \bar{q}q \rangle$. But this is not a true vacuum expectation value; instead, it is the matrix element of the operator $\bar{q}q$ in the background field of the \bar{b} quark. The change in the (dynamical) mass of the light quark in this bound state is somewhat reminiscent of the energy shift of an electron in the Lamb shift, in that both are consequences of the fermion being in a bound state rather than propagating freely. Similarly, it is important to use the equations of motion for confined quarks and gluon fields when analyzing current correlators in QCD, not free propagators, as has often been done in traditional analyses of operator products. Since the distance between the quark and antiquark cannot become arbitrarily large, one cannot create a quark condensate which has uniform extent throughout the universe. Thus in a fully self-consistent treatment of the bound state, this phenomenon occurs in the background field of the \bar{b} -quark, whose influence on light-quark propagation is primarily concentrated in the far infrared and whose presence ensures the manifestations of light-quark dressing are gauge invariant.

In the case of the pion one finds that the vacuum quark condensate that appears in the Gell Mann-Oakes Renner formula, is, in fact, a chiral-limit value of an ‘in-pion’ condensate [30]. This condensate is no more a property of the “vacuum” than the pion’s chiral-limit leptonic decay constant. One can connect the Bethe-Salpeter formalism to the light-front formalism, by fixing the light-front time τ . This then leads to the Fock state expansion. In fact, dynamical CSB in the light-front formulation, expressed via ‘in-hadron’ condensates, can be shown to be connected with sea-quarks derived from higher Fock states. This solution is similar to that discussed in Ref. [72]. Moreover, Ref. [75] establishes the equivalence of all three definitions of the vacuum quark condensate: a constant in the operator product expansion, [76, 77] via the Banks-Casher formula, [78] and the trace of the chiral-limit dressed-quark propagator.

Acknowledgments

Invited talk, presented at the Gribov-80 Memorial Workshop on Quantum Chromodynamics and Beyond, held at the Abdus Salam International Centre for Theoretical Physics, Trieste, Italy. I am grateful to Julia Nyiri and Yuri Dokshitzer for their invitation to this meeting, and I thank all of my collaborators whose work has been cited in this report. This research was supported by the Department of Energy, contract DE-AC02-76SF00515. SLAC-PUB 14265.

-
- [1] S. J. Brodsky, I. Schmidt and J. J. Yang, *Phys. Rev. D* **70**, 116003 (2004) [arXiv:hep-ph/0409279].
 - [2] I. Schienbein, J. Y. Yu, C. Keppel, J. G. Morfin, F. I. Olness and J. F. Owens, arXiv:0806.0723 [hep-ph].
 - [3] F. Arleo, S. J. Brodsky, D. S. Hwang and A. M. Sickles, *Phys. Rev. Lett.* **105**, 062002 (2010) [arXiv:0911.4604 [hep-ph]].
 - [4] F. Arleo, S. J. Brodsky, D. S. Hwang and A. M. Sickles, arXiv:1006.4045 [hep-ph].
 - [5] S. J. Brodsky and A. Sickles, *Phys. Lett. B* **668**, 111 (2008) [arXiv:0804.4608 [hep-ph]].
 - [6] S. S. Adler *et al.* [PHENIX Collaboration], *Phys. Rev. Lett.* **91**, 172301 (2003) [arXiv:nucl-ex/0305036].
 - [7] S. J. Brodsky, D. S. Hwang and I. Schmidt, *Phys. Lett. B* **530**, 99 (2002) [arXiv:hep-ph/0201296].
 - [8] J. C. Collins, *Phys. Lett. B* **536**, 43 (2002) [arXiv:hep-ph/0204004].
 - [9] S. J. Brodsky, D. S. Hwang and I. Schmidt, *Nucl. Phys. B* **642**, 344 (2002) [arXiv:hep-ph/0206259].
 - [10] S. J. Brodsky, P. Hoyer, N. Marchal, S. Peigne and F. Sannino, *Phys. Rev. D* **65**, 114025 (2002) [arXiv:hep-ph/0104291].
 - [11] C. Adloff *et al.* [H1 Collaboration], *Z. Phys. C* **76**, 613 (1997) [arXiv:hep-ex/9708016].
 - [12] J. Breitweg *et al.* [ZEUS Collaboration], *Eur. Phys. J. C* **6**, 43 (1999) [arXiv:hep-ex/9807010].
 - [13] S. J. Brodsky, B. Pasquini, B. W. Xiao and F. Yuan, *Phys. Lett. B* **687**, 327 (2010) [arXiv:1001.1163 [hep-ph]].
 - [14] S. J. Brodsky, *Nucl. Phys. A* **827**, 327C (2009) [arXiv:0901.0781 [hep-ph]].
 - [15] J. Collins and J. W. Qiu, *Phys. Rev. D* **75**, 114014 (2007) [arXiv:0705.2141 [hep-ph]].
 - [16] D. Boer, S. J. Brodsky and D. S. Hwang, *Phys. Rev. D* **67**, 054003 (2003) [arXiv:hep-ph/0211110].
 - [17] D. Boer, *Phys. Rev. D* **60**, 014012 (1999) [arXiv:hep-ph/9902255].
 - [18] S. J. Brodsky, P. Hoyer, C. Peterson and N. Sakai, *Phys. Lett. B* **93**, 451 (1980).
 - [19] S. J. Brodsky, J. C. Collins, S. D. Ellis, J. F. Gunion and A. H. Mueller,
 - [20] B. W. Harris, J. Smith and R. Vogt, *Nucl. Phys. B* **461**, 181 (1996) [arXiv:hep-ph/9508403].
 - [21] M. Franz, M. V. Polyakov and K. Goeke, *Phys. Rev. D* **62**, 074024 (2000) [arXiv:hep-ph/0002240].
 - [22] S. J. Brodsky, B. Kopeliovich, I. Schmidt and J. Soffer, *Phys. Rev. D* **73**, 113005 (2006) [arXiv:hep-ph/0603238].
 - [23] S. J. Brodsky, G. P. Lepage and P. B. Mackenzie, *Phys. Rev. D* **28**, 228 (1983).
 - [24] S. J. Brodsky, G. T. Gabadadze, A. L. Kataev and H. J. Lu, *Phys. Lett. B* **372**, 133 (1996) [arXiv:hep-ph/9512367].
 - [25] S. J. Brodsky and H. J. Lu, *Phys. Rev. D* **51**, 3652 (1995) [arXiv:hep-ph/9405218].
 - [26] S. J. Brodsky, E. Gardi, G. Grunberg and J. Rathsman, *Phys. Rev. D* **63**, 094017 (2001) [arXiv:hep-ph/0002065].
 - [27] S. J. Brodsky, G. F. de Teramond and A. Deur, *Phys. Rev. D* **81**, 096010 (2010) [arXiv:1002.3948 [hep-ph]].
 - [28] S. J. Brodsky and R. Shrock, *Phys. Lett. B* **666**, 95 (2008) [arXiv:0806.1535 [hep-th]].
 - [29] S. J. Brodsky and R. Shrock, arXiv:0905.1151 [hep-th].
 - [30] S. J. Brodsky, C. D. Roberts, R. Shrock and P. C. Tandy, *Phys. Rev. C* **82**, 022201 (2010) [arXiv:1005.4610 [nucl-th]].
 - [31] S. J. Brodsky and B. T. Chertok, *Phys. Rev. D* **14**, 3003 (1976).
 - [32] V. A. Matveev and P. Sorba, *Lett. Nuovo Cim.* **20**, 435 (1977).
 - [33] S. J. Brodsky, C. R. Ji and G. P. Lepage, *Phys. Rev. Lett.* **51**, 83 (1983).
 - [34] R. G. Arnold *et al.*, *Phys. Rev. Lett.* **35**, 776 (1975).
 - [35] G. R. Farrar, K. Huleihel and H. y. Zhang, *Phys. Rev. Lett.* **74**, 650 (1995).
 - [36] S. J. Brodsky, F. J. Llanes-Estrada and A. P. Szczepaniak, *Phys. Rev. D* **79**, 033012 (2009) [arXiv:0812.0395 [hep-ph]].
 - [37] S. J. Brodsky, F. E. Close and J. F. Gunion, *Phys. Rev. D* **5**, 1384 (1972).
 - [38] S. J. Brodsky, F. E. Close and J. F. Gunion, *Phys. Rev. D* **8**, 3678 (1973).
 - [39] S. J. Brodsky, F. E. Close and J. F. Gunion, *Phys. Rev. D* **6**, 177 (1972).
 - [40] G. F. de Teramond and S. J. Brodsky, *Phys. Rev. Lett.* **94**, 201601 (2005) [arXiv:hep-th/0501022].
 - [41] G. F. de Teramond and S. J. Brodsky, *Phys. Rev. Lett.* **102**, 081601 (2009) [arXiv:0809.4899 [hep-ph]].
 - [42] S. J. Brodsky and G. F. de Teramond, arXiv:1009.4232 [hep-ph].
 - [43] S. J. Brodsky, G. de Teramond and R. Shrock, *AIP Conf. Proc.* **1056**, 3 (2008) [arXiv:0807.2484 [hep-ph]].
 - [44] D. W. Sivers, S. J. Brodsky and R. Blankenbecler, *Phys. Rept.* **23**, 1 (1976).
 - [45] S. J. Brodsky and M. Rijssenbeek, arXiv:hep-ph/0511178.
 - [46] J. W. Cronin, H. J. Frisch, M. J. Shochet, J. P. Boymond, P. A. Piroue and R. L. Sumner, *Phys. Rev. Lett.* **31**, 1426 (1973).
 - [47] D. Antreasyan, J. W. Cronin, H. J. Frisch, M. J. Shochet, L. Kluberg, P. A. Piroue and R. L. Sumner, *Phys. Rev. D* **19**, 764 (1979).
 - [48] R. Blankenbecler, S. J. Brodsky and J. F. Gunion, *Phys. Rev. D* **12**, 3469 (1975).
 - [49] E. L. Berger and S. J. Brodsky, *Phys. Rev. Lett.* **42**, 940 (1979).
 - [50] A. M. Sickles, *Nucl. Phys. A* **830**, 131C (2009) [arXiv:0907.4921 [nucl-ex]].

- [51] S. J. Brodsky and A. H. Mueller, Phys. Lett. B **206**, 685 (1988).
- [52] B. L. Ioffe, Phys. Lett. B **30**, 123 (1969).
- [53] S. J. Brodsky and H. J. Lu, Phys. Rev. Lett. **64**, 1342 (1990).
- [54] G. P. Zeller *et al.* [NuTeV Collaboration], Phys. Rev. Lett. **88**, 091802 (2002) [Erratum-ibid. **90**, 239902 (2003)] [arXiv:hep-ex/0110059].
- [55] S. J. Brodsky and D. S. Hwang, Nucl. Phys. B **543**, 239 (1999) [arXiv:hep-ph/9806358].
- [56] S. J. Brodsky, M. Diehl and D. S. Hwang, Nucl. Phys. B **596**, 99 (2001) [arXiv:hep-ph/0009254].
- [57] A. V. Belitsky, X. Ji and F. Yuan, Nucl. Phys. B **656**, 165 (2003) [arXiv:hep-ph/0208038].
- [58] J. C. Collins and A. Metz, Phys. Rev. Lett. **93**, 252001 (2004) [arXiv:hep-ph/0408249].
- [59] J. C. Collins, Acta Phys. Polon. B **34**, 3103 (2003) [arXiv:hep-ph/0304122].
- [60] S. J. Brodsky and M. Karliner, Phys. Rev. Lett. **78**, 4682 (1997) [arXiv:hep-ph/9704379].
- [61] S. J. Brodsky and S. Gardner, Phys. Rev. D **65**, 054016 (2002) [arXiv:hep-ph/0108121].
- [62] P. Hoyer, M. Vanttinen and U. Sukhatme, Phys. Lett. B **246**, 217 (1990).
- [63] J. Badier *et al.* [NA3 Collaboration], Phys. Lett. B **104**, 335 (1981).
- [64] M. J. Leitch *et al.* [FNAL E866/NuSea collaboration], Phys. Rev. Lett. **84**, 3256 (2000) [arXiv:nucl-ex/9909007].
- [65] J. C. Anjos, J. Magnin and G. Herrera, Phys. Lett. B **523**, 29 (2001) [arXiv:hep-ph/0109185].
- [66] A. Ocherashvili *et al.* [SELEX Collaboration], Phys. Lett. B **628**, 18 (2005) [arXiv:hep-ex/0406033].
- [67] R. Vogt and S. J. Brodsky, Phys. Lett. B **349**, 569 (1995) [arXiv:hep-ph/9503206].
- [68] G. Bari *et al.*, Nuovo Cim. A **104**, 1787 (1991).
- [69] J. Pumplin, H. L. Lai and W. K. Tung, Phys. Rev. D **75**, 054029 (2007) [arXiv:hep-ph/0701220].
- [70] V. M. Abazov *et al.* [D0 Collaboration], Phys. Rev. Lett. **102**, 192002 (2009) [arXiv:0901.0739 [hep-ex]].
- [71] P. P. Srivastava and S. J. Brodsky, Phys. Rev. D **66**, 045019 (2002) [arXiv:hep-ph/0202141].
- [72] A. Casher and L. Susskind, Phys. Rev. D **9**, 436 (1974).
- [73] S. J. Brodsky and R. Shrock, arXiv:0803.2541 [hep-th].
- [74] S. J. Brodsky and R. Shrock, arXiv:0803.2554 [hep-th].
- [75] K. Langfeld, H. Markum, R. Pullirsch, C. D. Roberts and S. M. Schmidt, Phys. Rev. C **67**, 065206 (2003) [arXiv:nucl-th/0301024].
- [76] K. D. Lane, Phys. Rev. D **10**, 2605 (1974).
- [77] H. D. Politzer, Nucl. Phys. B **117**, 397 (1976).
- [78] T. Banks and A. Casher, Nucl. Phys. B **169**, 103 (1980).